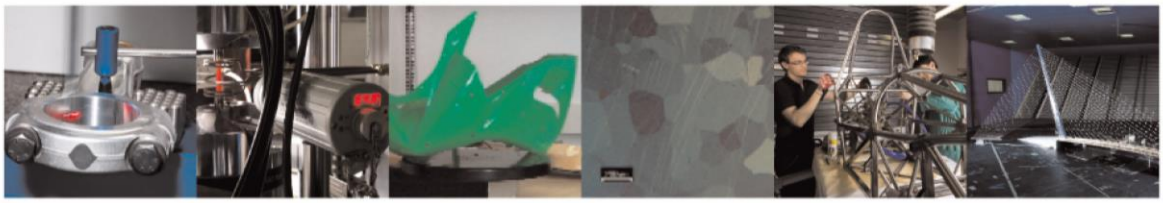

# Design and functional testing of a novel balloon-expandable cardiovascular stent in CoCr alloy produced by selective laser melting

Valentina Finazzi, Ali Gökhan Demir, Carlo Alberto Biffi, Francesco Migliavacca, Lorenza Petrini, Barbara Previtali

This is a post-peer-review, pre-copyedit version of an article published in Journal of Manufacturing Processes. The final authenticated version is available online at: http://dx.doi.org/10.1016/j.jmapro.2020.03.060



DIPARTIMENTO DI MECCANICA ■ POLITECNICO DI MILANO
via G. La Masa, 1 ■ 20156 Milano ■ EMAIL (PEC): pecmecc@cert.polimi.it
http://www.mecc.polimi.it
Rev. 0

# Design and functional testing of a novel balloon-expandable cardiovascular stent in CoCr alloy produced by selective laser melting

Valentina Finazzi[a,b], Ali Gökhan Demir[a*], Carlo Alberto Biffi[c], Francesco Migliavacca[d], Lorenza Petrini[b], Barbara Previtali[a]

[a]*Department of Mechanical Engineering, Politecnico di Milano, Via La Masa 1, 20156 Milan, Italy*
[b]*Department of Civil and Environmental Engineering, Politecnico di Milano, Piazza Leonardo da Vinci 32, 20133 Milan, Italy*
[c]*National Research Council - Institute of Condensed Matter Chemistry and Technologies for Energy, CNR ICMATE, Via Previati 1E, 23900 Lecco, Italy*
[d]*Laboratory of Biological Structure Mechanics, Department of Chemistry, Materials and Chemical Engineering 'Giulio Natta', Politecnico di Milano, Piazza Leonardo da Vinci 32, 20133 Milan, Italy*

*Corresponding author: aligokhan.demir@polimi.it

**Design and functional testing of a novel balloon-expandable cardiovascular stent in CoCr alloy produced by selective laser melting**

Valentina Finazzi[a,b]
Ali Gökhan Demir[a*]
Carlo Alberto Biffi[c]
Francesco Migliavacca[d]
Lorenza Petrini[b]
Barbara Previtali[a]

[a]*Department of Mechanical Engineering, Politecnico di Milano, Via La Masa 1, 20156 Milan, Italy*
[b]*Department of Civil and Environmental Engineering, Politecnico di Milano, Piazza Leonardo da Vinci 32, 20133 Milan, Italy*
[c]*National Research Council - Institute of Condensed Matter Chemistry and Technologies for Energy, CNR ICMATE, Via Previati 1E, 23900 Lecco, Italy*
[d]*Laboratory of Biological Structure Mechanics, Department of Chemistry, Materials and Chemical Engineering 'Giulio Natta', Politecnico di Milano, Piazza Leonardo da Vinci 32, 20133 Milan, Italy*
*Corresponding author: aligokhan.demir@polimi.it

## Abstract

Selective Laser Melting (SLM) is a promising technology for the realization of patient-specific medical implants, due to the intrinsic potential in the realization of complex geometries. The present work analyses the production of balloon-expandable stents in cobalt-chromium alloy with a novel mesh which is realized using an industrial SLM system. A stent mesh, optimized for SLM process, was designed, produced, finished and functionally tested by balloon expansion. An electropolishing treatment was used to clean the stent surface from sintered particles and to improve the surface finishing. Roughness measurements were carried out on stents both in the as-built and the electropolished conditions, while mechanical properties were evaluated by tensile testing with dogbone specimens, produced with the same parameters of the stents and having comparable dimensions. Finally, the expansion behaviour of the CoCr stents, both in as-built and electropolished conditions, was assessed using a balloon catheter and measuring the diameter variation as a function of inflation pressure. The results confirm that SLM produced stents can be successfully balloon expanded without damaging their characteristic mesh.

**Keywords:** Stents; biomedical devices; design for additive manufacturing; electropolishing; micro additive manufacturing

## 1. Introduction

In industrialised countries cardiovascular diseases are the main cause of mortality [1] and a high number of patients requires treatment for occlusions of blood vessels. Percutaneous coronary intervention (PCI) is nowadays the gold

standard treatment, and it foresees, after that the vessel capacity is restored by inflating a balloon the implantation of a stent in order to maintain the lumen open in the months after the intervention. Stents can be produced using metals or polymers, and their use depends on the type and position of the occlusion. Stents usually have a polymeric coating which contains drugs to locally treat inflammations, as in the case of drug eluting stents (DES) [2]. Polymers can be more suitable to produce biodegradable devices [3], while metals have mechanical properties which are more appropriated to sustain the high loads present in the vessels, which can be both static and cyclic [4]. In particular, cobalt-chromium alloys are nowadays the most used material for balloon-expandable stents, since they allow to decrease the strut thickness exploiting their high strength [5].

The most common manufacturing route for metal stents is micro laser cutting of tubular precursors [6]. Using selective laser melting (SLM) the production chain can be reduced, substituting tube drawing and micro laser cutting within a single manufacturing step. Moreover, the new manufacturing process removes the constraints of a tubular precursor and the presence of oxides typical of laser cut stent surfaces [7], since SLM process works in inert atmosphere. At the same time, the realization of new geometries could be investigated, such as stents for lesions in correspondence of bifurcation sites or for vessels with high tortuosity, which are not well represented by the rectilinear axis of tubes [8]. Other advantages to be considered when comparing laser cutting to additive technologies are the material waste and the parallel production. In stent production with laser cutting, the material cut to create the mesh is treated as scrap [9], while SLM systems have the possibility to recycle and reuse the unmelted powder.

Additive manufacturing has been studied to produce stents in polymeric materials [10–15]. Only recently the use of additive manufacturing with metallic powders is gaining attention. In particular, works by Demir et al. [16], Wessarges et al [17], and Wen et al. [18] demonstrated the feasibility of SLM process to realize stent geometries, using respectively cobalt-chromium, stainless steel and pure zinc powders. The production of stents via SLM is still highly challenging mainly due to the dimensional limits of the process employing industrial machines. The strut size of metallic stents (60-150 μm) is comparable with laser spot (30-100 μm) and powder grain size (10-50 μm) [16]. On the other hand, the use of industrial SLM systems can be considered intrinsically safer as opposed

to micro-SLM systems that employ smaller particle sizes (<10 μm), which require a higher degree of safety regulations due to increased inhalation issues and flammability [19].

Many studies on the use of lattice structures in SLM process were carried out [20–25] and considerations on such features can be applied for the realization of stents, given the geometrical similarities between such components. The use of pulsed-wave emission was found to be more convenient to obtain small features allowed by smaller melt pools [26–28]. Regarding the use of CoCr powders to produce biomedical implants with SLM process, in literature studies can be found on biocompatibility [29–31] and mechanical properties analyses [32–34], also taking into consideration interactions with body fluids [35,36] and chemical post-processing [37]. However, balloon-expandable stents with strut sizes comparable to the conventional ones still require further investigations from the production cycle perspective. Indeed, the SLM process parameters play a crucial role on the feasibility of producing stents.

Another important issue regards the surface finishing of the SLM produced medical devices. The high roughness which is a characteristic of the SLM process needs to be improved especially for small devices. The surface roughness profile is a combination of effects concerning the melt pool shape and the presence of sintered particles [38]. For biomedical applications, $R_a$ values below 0.5 μm are strictly required, so a finishing surface process is required. The surface post-processing of SLM produced stents is a challenging task, due to the complex forms. Chemical, electrochemical and abrasive flow machining are some of the options used for surface finishing of SLM produced components [39][40]. Laser cut stents are chemically and electrochemically etched for achieving the final shape, size and surface roughness [41,42]. The feasibility of using the conventional electropolishing method on SLM produced surfaces needs to be addressed.

Additive manufacturing (AM) of stents by SLM provides several challenges concerning manufacturing, finishing, and material characterisation steps. Moreover, the correct functioning of the devices relies highly on the use of design rules for AM. In this work, for the first time, to authors' knowledge, the feasibility of producing metallic stents via AM is addressed by discussing all the necessary steps: from the additive manufacturing process details, to the finishing procedure and testing aspects. In particular, a novel mesh for a cardiovascular stent in CoCr alloy is proposed and its design is parametrically controlled in relation to the layer thickness, while the strut thickness

is varied to test its influence on the geometrical accuracy. Material mechanical characterization is carried out using tensile specimens manufactured with the same process and having the same dimensions of the stent strut. Electrochemical polishing is applied, and the obtained strut thickness is characterized. Finally, stents are functionally characterized by ballooned catheter expansion.

## 2. Materials and methods

### 2.1. Design of the stent mesh

SLM provides a high geometrical freedom, but at the same time it has limits related to inclinations, dimensions and heat dissipation requirements. A parametric mesh, designed by Finazzi et al. [8], was used for the present study. The build direction corresponds to the axis of the stent and the main parameter of such design is the powder layer thickness. Every vertical distance between the struts and the strut thickness itself are multiple of the powder layer thickness. The final dimension was determined equal to 30 μm as layer thickness, which provided sufficient detail and compatibility with the conventional powder sizes for micro applications (15-45 μm) allowing to minimize the stair-case effect typical of the SLM process [43]. SLM design rules on inclinations and feature dimensions were followed as well, in order to realize a support-free stent [8]. The closed-cell geometry was chosen to avoid supports and corrugated links were used to give flexibility. The designed stents were drawn from a tube, wrapping the 2D mesh (Figure 1.a) to obtain a 3D model. The parametric design consisted of dimensional choices as multiples of the layer thickness (z) to ensure the geometrical fidelity.

Strut size combined with manufacturing process may affect the material mechanical properties [44,45]. In order to test the mechanical properties of the SLM produced thin struts, tensile specimens were designed with a 6 mm gauge length and the same nominal thickness of the stent struts (t). As seen in Figure 1.b, the tensile specimens were produced with lateral supports to sustain the upper gripper section during the SLM process. The lateral supports were removed prior to the tensile test.

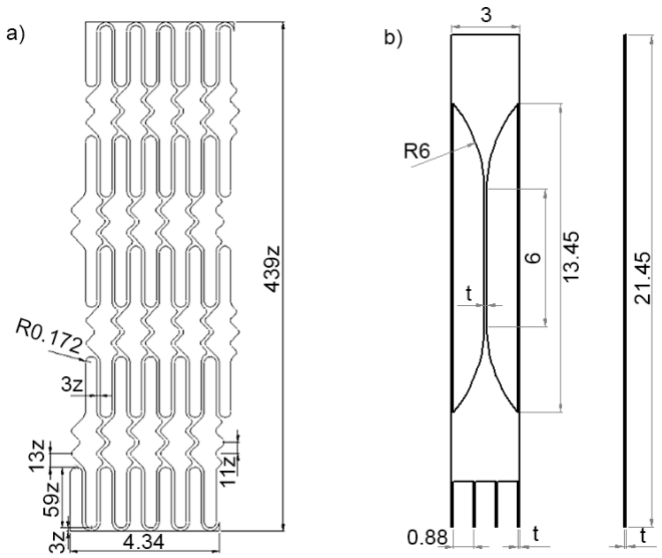


Figure 1. a) Stent mesh optimized for SLM production and b) drawing of the mini tensile specimens. The parametric designs are shown in relation to the multiples of the layer thickness (z) and the nominal strut thickness (t).

### 2.2. CoCr powder

A CoCr powder from LPW Technology (Cheshire, UK) was used for the study. Such CoCr alloy has chemical composition similar to ASTM F75 requirements and powders with similar composition were proved to be suitable for biomedical applications [46]. The nominal composition is reported in Table 1. The powder, gas atomized under Ar, has a size distribution between D10 at 20 µm and D90 53 µm with a spherical morphology (see Figure 2). Powder apparent density was 5.04 g/cm3, whereas the solid density is 8.3 g/cm3.

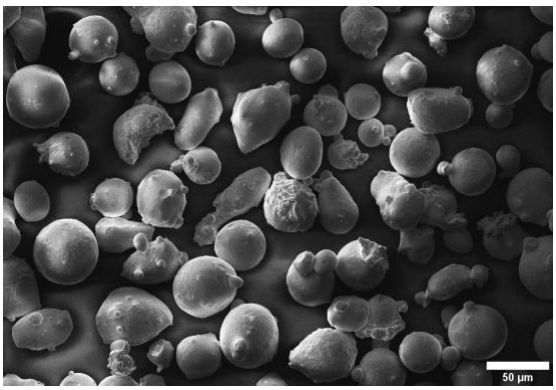


Figure 2. SEM image of the CoCr powder used in the present work.

Table 1. Nominal chemical composition of the CoCr powder declared by the producer; percentage expressed in weight percentage (wt. %).

| Cr | Mo | Co | O | Si | Mn | Fe | Ni | N | W | Al | Ti |
|---|---|---|---|---|---|---|---|---|---|---|---|
| 27-30 | 5-7 | bal. | <0.10 | <1.00 | <1.00 | <0.75 | <0.50 | <0.25 | <0.20 | <0.10 | <0.1 |

### 2.3. Selective laser melting system

An industrial SLM system (Renishaw AM250, Stone, UK) was used for this work. The system is equipped with a 200 W single mode fibre laser (R4 from SPI, Southampton, UK) and an optical chain which provides a 75 μm beam diameter in the focus position (f=0 mm). The laser is run in pulsed mode (PW) by power modulation to achieve μs-long pulses. The system works under controlled atmosphere. Prior to the build process, the processing chamber is filled with Ar, with 15 mbar overpressure, and the during the process the oxygen content is maintained below 1000 ppm. A Reduced Built Volume (RBV) platform was used on the AM250 system, which limits the build chamber to 78x78x50 $mm^3$ while employing limited quantity of powder (<3 kg).

## 3. Experimental

### 3.1. Selective laser melting parameters

The process parameters were selected starting from a previous work on the same alloy [16]. According to functioning principle of the modulated PW emission the scanner moves the laser beam on the desired trajectory with a continuous motion. The laser is modulated to release pulses with a determined peak power (P) for a fixed time interval (the pulse duration, $t_{on}$) of 120 μs [47]. On a scanned vector line, laser exposure points were separated by a point distance ($d_p$), which is controlled by the pulsation frequency and the scan speed employed. Once a certain scan vector has been executed, the beam jumps to the consecutive vector lines, which are separated by a line distance ($d_l$). Point and line distances were kept equal, which was found to be advantageous for thin struts [48] at 40 μm. In particular, a concentric scan strategy was employed scanning from inside towards outside of each contour. The positioning of the pulses in a concentric scan strategy along with the pulsed emission profile are illustrated in Figure 3.a and b. Since point and line distances are comparable to the strut size, the nominal strut thickness has an effect on the number of concentric trajectories and hence on the number of pulses per strut. Accordingly, the nominal strut thickness was considered a process parameter and set as 90 and 120 μm. Figure 4 shows the disposition of the laser pulses and scan trajectories as a function of the nominal strut thickness. It can be seen that the trajectories are calculated differently for the two strut thicknesses, which can have an important impact on the final dimensions and geometrical accuracy.

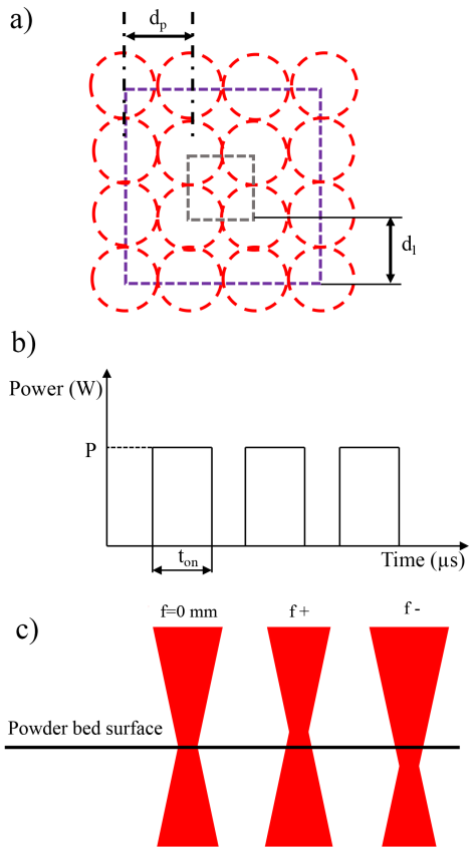


Figure 3. Schematic representation of the effect of the process parameters. a) The definition of point ($d_p$) and line distances ($d_l$) in concentric scan strategy, where the grey dashed line shows the inner scan contour, purple dashed line shows the outer scan contour. b) Peak power (P) and pulse duration ($t_{on}$) control. c) The propagation of the laser beam and the influence of the focal position (f).

Layer thickness (z) determines the distance among each slice applied to the digital model of the part to be built. Moreover, it is an important factor concerning the surface roughness along the build direction as well as the formation of the so-called staircase effect. Smaller layer thicknesses are advantageous for the production of the stents as it improved the geometrical fidelity to the digital model. However, the layer thickness should be chosen also as a function of the powder size distribution in order to accommodate all the particle sizes in the layer. According to Spierings et al, the process should settle to the effective layer thickness due to differences of the powder and solid densities [49]. In the present work, layer thickness was chosen at 30 µm, where an effective layer thickness of approximately 50 µm after 10 layers is expected. Hence, most of the powder size distribution is expected to be accommodated within each layer. Focal position of the optical chain can be controlled to have the minimum beam size on the powder bed surface (f=0 mm), above (f+) or below (f-) as shown in Figure 3.c. Throughout the experiments, the focal point was kept on the power bed surface (f=0 mm) employing the smallest

beam size. No beam compensation was applied to the nominal struts size. For larger components, different sets of parameters are commonly employed for down-skin and up-skin regions. Down-skin regions correspond to downfacing surfaces with respect to the build direction suspended on the powder bed, which can be characterized by higher surface roughness [50]. Up-skin regions correspond to surfaces that face upwards with respect to the build direction, where different sets of parameters can be used to achieve a better surface finish. The down-skin regions are commonly those that are below the minimum inclination angle (i.e. commonly 45° for CoCr), which may also require support structures. Up-skin regions are also found at a similar inclination angle, this time for upward facing surfaces. The size of the stent struts required an overall parameter choice in order to ensure the geometrical fidelity required. Hence, no up-skin or down-skin strategies were employed. Stents were analysed in as-built and electropolished conditions. Laser trajectories and parameters, as well as slicing and layer thickness, were assigned with Magics 19 from Materialise (Leuven, Belgium). Laser exposure positions were viewed using QuantAM (Renishaw, Stone, UK) as seen Figure 4. Table 2 summarizes the details of the experimental plan.

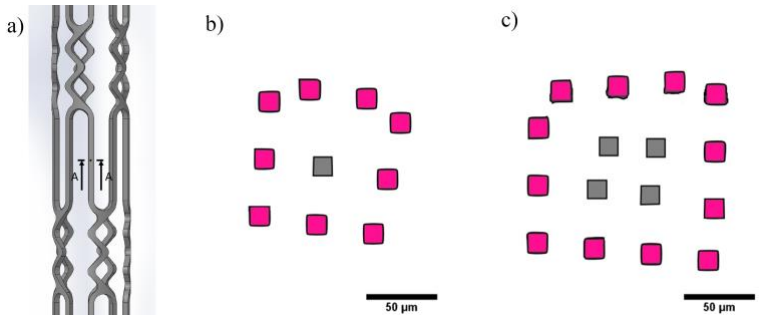


Figure 4. Influence of the strut nominal thickness on the number of pulses in a scanned layer. a) Designed stent prototype and A-A section line depicting the layer in which the assigned position of the laser pulses are viewed belonging to a strut with b) 90 µm thickness and c) 120 µm thickness. Grey squares depict the pulses of the inner scan contour, pink square depict the pulses of the outer scan contour.

Table 2. Details of the experimental plan.

| **Fixed parameters** | **Value** |
|---|---|
| Strategy | Concentric scanning |
| Focal position, $f$ (mm) | 0 |
| Point distance, $d_p$ (µm) | 40 |
| Line distance, $d_l$ (µm) | 40 |
| Layer thickness, $z$ (µm) | 30 |
| Pulse duration, $t_{on}$ (µs) | 120 |
| **Varied parameters** | **Levels** |
| Peak power, $P$ (W) | 40; 50 |
| Nominal strut thickness, $t$ (µm) | 90; 120 |

### 3.2. Electrochemical polishing

Electrochemical polishing was applied after the SLM process for improving the surface quality. The electrolytic solution was composed of 50 vol% phosphoric acid, 45 vol% of sulfuric acid, and 5 vol% of distilled water. The stents were connected to the positive terminal of the current generator, while a stainless-steel cathode was connected to the negative one. Temperature was kept constant at 15 °C and the voltage applied was 12 V for 2.5 minutes. The total immersion time was divided in 3 steps, having durations of 1.5 min, 30 s and 30 s, respectively. Between the immersion steps, the stents were cleaned by ultrasonication in ethyl alcohol.

### 3.3. Characterization

#### 3.3.1. Surface quality

Images of stents before and after electropolishing were acquired using a scanning electron microscopy (SEM, EVO-50 and LEO-1430 from Carl Zeiss, Oberkochen, Germany), to observe geometry accuracy and surface morphology. Surface roughness of the produced stents was measured by means of focus variation microscopy, using InfiniteFocus from Alicona Imaging GmbH (Graz, Austria). A 10X objective was used, with 0.3 µm vertical resolution and 2 µm lateral resolution. For each condition 5 replications were measured 3 times.

#### 3.3.2. Density and geometry

Micro X-ray Computed Tomography (CT), NSI X-25 from North Star Imaging (Rogers, MN, USA) was used to inspect porosity and internal defects before and after electropolishing. As-built stents were acquired with a voxel size of 3.9 x 3.9 x 3.9 $\mu m^3$, while a voxel size of 3.6 x 3.6 x 3.6 $\mu m^3$ was obtained for electropolished stents. From the CT images of the stents, transversal cross-sections were extracted at regular intervals given by the voxel size and analysed. The strut thickness was evaluated as an average value for each stent using images taken with an optical microscope with 200X magnification (UM 300I, Echo Lab, Paderno Dugnano, MI, Italy) and taking 10 measurements in different regions of the stent, using an image processing software (ImageJ, U.S. National

Institutes of Health, Bethesda, Maryland, USA). Dimensional error of the strut thickness ($e_t$) was calculated using the following equation

$$e_t = t_m - t \quad (1)$$

where t is the nominal thickness given by the digital model and $t_m$ is the measured thickness. It was noted in the experimental work that the strut section deviated to a circular shape in as-built and electropolished states, which required a measure of the section change. The strut section difference ($\Delta A$) was also calculated from the measurements as

$$\Delta A = A_m - A \quad (1)$$

where A is the nominal strut section and $A_m$ is the strut measured section calculated.

#### 3.3.3. Material properties

The mechanical behaviour of the SLM samples was characterised with tensile tests performed with a dynamic mechanical analyser Q800 from TA Instruments (New Castle, DE, USA), which can apply a maximum static force of 18 N. Tensile specimens were clamped at the extremities and the testing was done under strain control, ranging from 0.4%, a pre-load to remove slack, to 15%. Tests were carried out at ambient conditions. For each condition four replications were tested. The real resistant section of the specimens was measured from the SEM images prior to the tensile tests. Ten measurements for each specimen were taken, five from the front view and five from the lateral view of the gauge length.

#### 3.3.4. Expansion behaviour

The stents were expanded using a balloon catheter (NC Sprinter RX Noncompliant Rapid Exchange Balloon Dilatation Catheter, Medtronic, Dublin, Ireland) and a manual inflation device (BasixCOMPAK, Merit Medical Systems, South Jordan, UT, USA). Figure 5.a shows a schematic drawing of the setup for the tests. To guarantee equal conditions along all the stent external surfaces, a home-made expansion platform was used to keep the stent mounted on the balloon catheter free from external constraints and it is shown in Figure 5.b. Images during stent

expansion were taken using a stereo microscope SM 353 H from echoLAB (Cormano, Italy) with a 0.65X magnification and 8.56 micron/pixel resolution. In order to enhance the contrast of the images, blue food colorant was added to water and injected inside the catheter. All the stents were expanded with an increase of the balloon pressure from 0 to 8 bar and videos were acquired. At each pressure step of 1 bar, the stent external diameter was measured in the central portion of the device. Three measurements were taken at each position for each pressure value. Expansion ratio was also calculated from the measurements with the following equation:

$$r_x = d(p)/d_0 \quad (1)$$

where d is the diameter measured at a given pressure (p), and $d_0$ is the initial diameter.

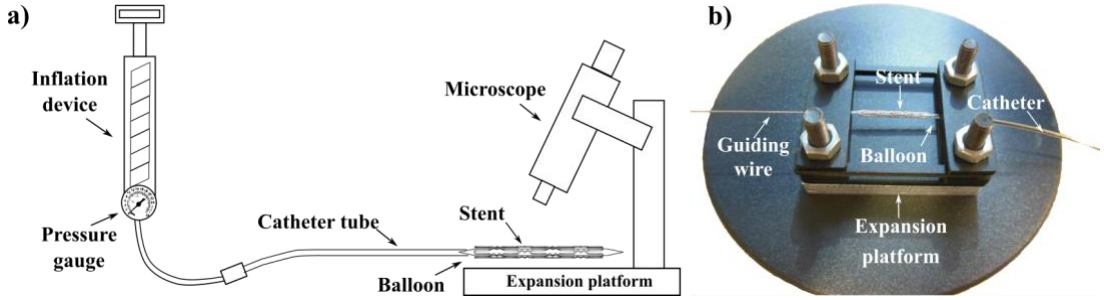


Figure 5. a) Schematic outline of expansion tests. b) Home-made expansion platform.

## 4. Results

### 4.1. Surface quality

Figure 6 shows the stents and tensile specimens on the build plate. No macro defects were observed, confirming stable build conditions with a rather conservative nesting on the build plate. The SEM images of the stents in the as-built condition and after electropolishing are shown in Figure 7. In the as-built condition, the mesh geometry appeared intact, while the surface showed the typical aspects of SLM parts, such as solidified melt pools and sintered particles (see Figure 7.a). In Figure 7.b it is visible how the electropolishing process allowed the removal of all the sintered particles and decreased the strut size, yet without excessively altering the cell shape. Figure 8 shows the stent link zones as a function of process parameters in as-built and electropolished conditions. All the as-built stents exhibited a higher strut thickness than the nominal one, since no beam compensation was applied,

decision based on the small dimensions which were involved. Stents realised with higher peak power showed larger strut size, due to the higher energy input, which causes a larger melt pool. Such difference in size appears to be reduced after the electrochemical polishing step.


Figure 6. Stents and tensile specimens in as-built conditions on the build plate.

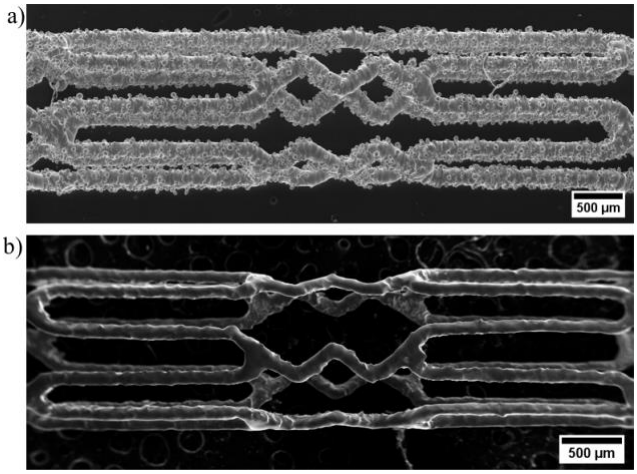


Figure 7. SEM image of a produced stent a) in the as-built condition and b) after electropolishing (P=50W, t=90 µm).

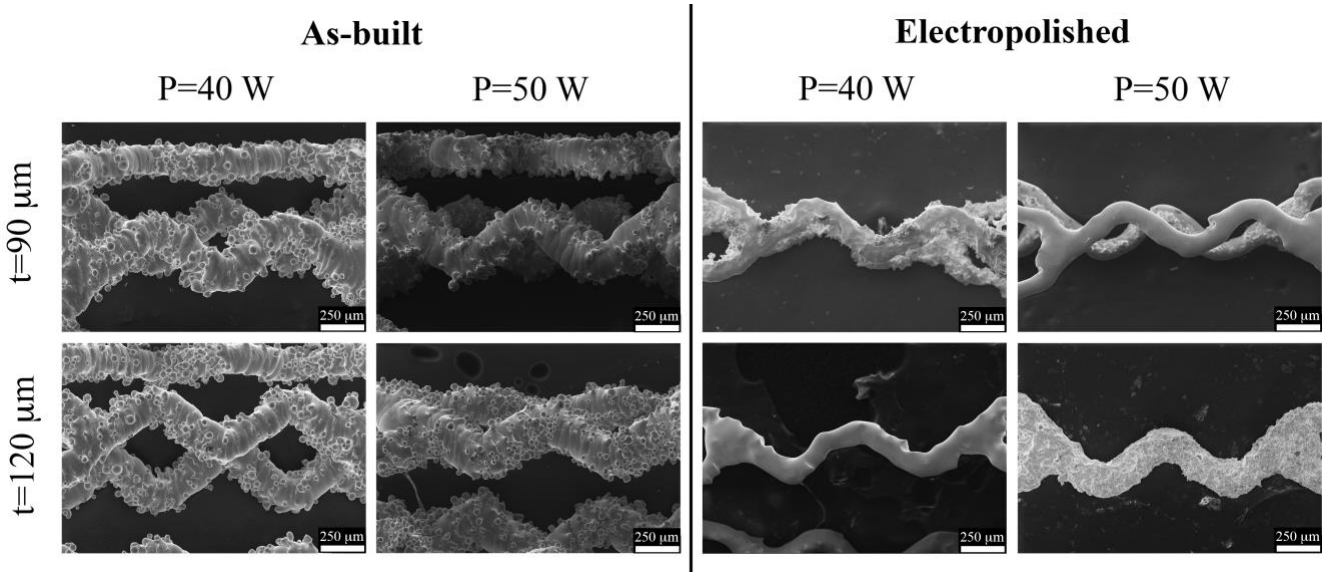


Figure 8. SEM image of produced stent in the as-built condition and after electropolishing as a function of process parameters.

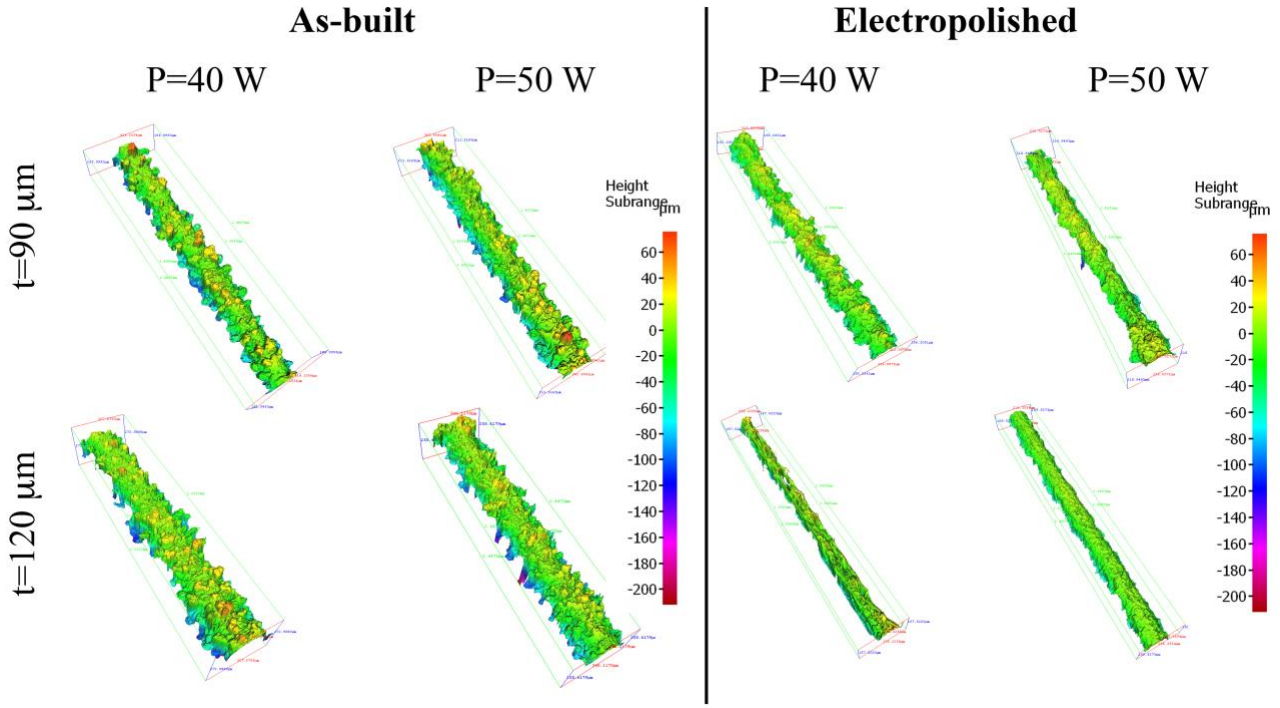


Figure 9. Surface morphology of stent struts in the as-built condition and after electropolishing.

Figure 9.a shows focus variation microscopy image of a strut in as-built condition, while Figure 9.b shows a strut after electropolishing. It appears that with electropolishing, all the sintered particles were removed; the thickness and roughness were reduced, as well. In terms of surface roughness parameters, no significant difference was observed between different power and nominal thickness groups. Figure 10 reports the roughness parameters in as-built and electropolished conditions. In particular, average roughness $R_a$ decreased from 8.4 µm to 2.2 µm, root mean square roughness $R_q$ from 9.3 µm to 3 µm, while mean roughness depth $R_z$ from 37.8 µm to 12.9 µm. The achieved values indicate an important reduction of the surface roughness. However, the further reduction of $R_a$ is required to achieve the surface finish conventionally required for stents ($Ra<0.5$ µm). Prolonged exposure to electrochemical etching was found to excessively reduce the strut thickness. Further improvement of the surface quality can be addressed through the use of different etching solutions, as well as combining different finishing steps such as abrasive and electrochemical [40].

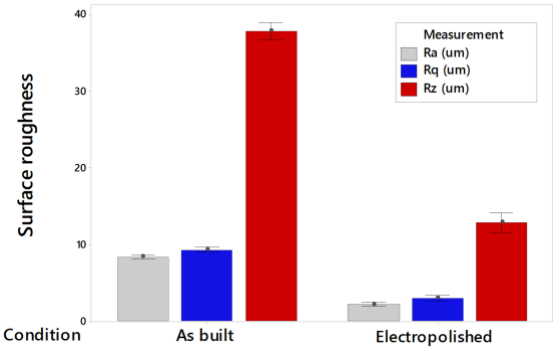


Figure 10. Average roughness ($R_a$), root mean square roughness ($R_q$) and mean roughness depth ($R_z$) of SLM stents in the as-built condition and electropolished (error bars indicate standard error).

### 4.2. Density and geometry

Reconstruction of the stents in as-built and electropolished condition is reported in Figure 11.a-b, respectively. From the cross-sections (Figure 10.c-d), it can be seen that the stents are fully dense, and no appreciable porosity is present, before and after electropolishing. Moreover, the obtained geometry appears to be different from the nominal one. In fact, the strut section is circular instead of exhibiting the typical shape of the tube wall. Such difference is attributed to the as laser spot and melt pool geometries, The strut shape remained circular after the electropolishing stage. This indicates that the electropolishing acts conformal to the initial shape of the strut and reduces the strut size homogenously.

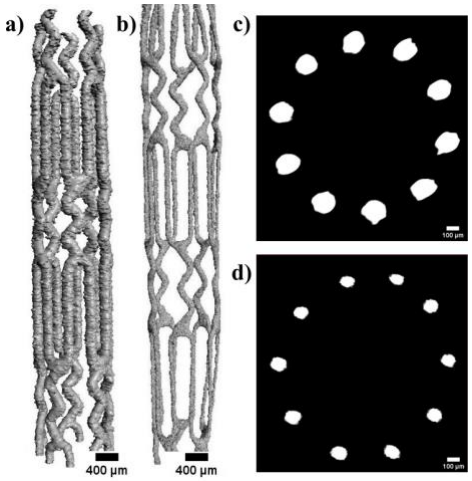


Figure 11. Micro CT reconstructions (a and b) and cross-sections (c and d) of SLM stents in as-built condition (a and c) and after electropolishing (b and d) (P=50W, t=90 µm).

### 4.3. Strut thickness and dimensional error

Dimensional error ($e_t$) on strut thickness in as-built and electropolished conditions was evaluated and the corresponding trends are reported in Figure 12.a. The thickness of the struts are larger than the nominal as

expected, due to the absence of beam compensation. It can be noticed that the power level did not induce a notable change of the strut thickness in the as-built stents. The nominal strut thickness was the dominant factor on generating a larger dimensional error in the as-built condition. After electropolishing instead, the obtained thicknesses were similar to the nominal one. In all conditions the electropolishing produced a thickness reduction of approximately 75 µm, when surface cleaning was achieved at the desired level.. Figure 12.b shows the strut section difference in as-built condition and after electropolishing. It can be observed that after electropolishing the strut size was reduced below its nominal value due to the change of the section geometry. It can be concluded that the section area plays a more critical role in the mechanical behaviour of the stent. Hence, in order to maintain the desired section size, the combination of electrochemical polishing with a larger nominal strut thickness was found to be more adequate.

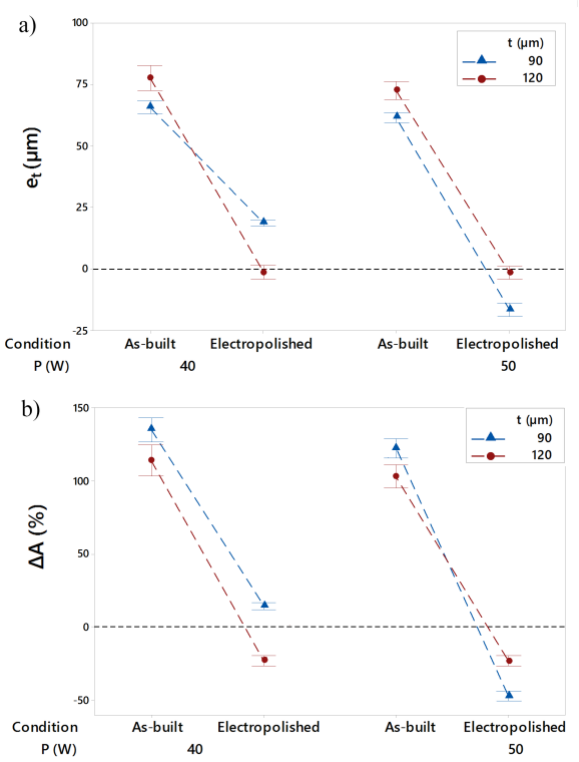


Figure 12. a) Strut thickness error ($e_t$) and b) strut section change for stents in as-built and electropolished conditions (error bars indicate standard error).

### 4.4. Material properties

Figure 13.a shows typical engineering stress-strain curves for different process parameters, while the resulting mechanical properties are reported in Figure 13.b. For all conditions, elastic modulus (E) and yield strength (YS)

could be evaluated. For specimens with 90 μm thickness, also ultimate tensile strength (UTS) and the corresponding elongation at fracture ($\varepsilon_f$) could be evaluated, while for the specimens with nominal thickness of 120 μm it was not possible to evaluate UTS and $\varepsilon_f$, since the maximum static force of the machine was reached. The elastic modulus showed a minimum average value for the combination t=120μm and P=50W, while the maximum was for t=90μm and P=40W. In general, it seems that higher peak power and higher thickness lead to lower elastic modulus. In the case of specimens with 90 μm nominal thickness the increase of the laser peak power enhances both the $\varepsilon_f$ and UTS.

The mechanical properties of the SLM produced samples are summarized in Table 3 and compared to the wrought alloy with an equivalent chemical composition (L605). The results in terms of elastic modulus are particularly interesting, since common values for CoCr alloys are one order of magnitude higher, both for classical technologies and SLM produced macro specimens [51]. Considering that the micro CT measurements showed no internal porosity, the lower elastic modulus can be attributed to the combination of the SLM produced microstructure and the size effect. Such results require further studies for a better understanding of the underlying phenomenon, as well as exploitation for also load bearing orthopaedic applications that may require lower elastic modulus. Overall, the results confirm that the mechanical properties are comparable to the material conventionally produced and expected to allow balloon expansion without causing failures for stenting applications [52].

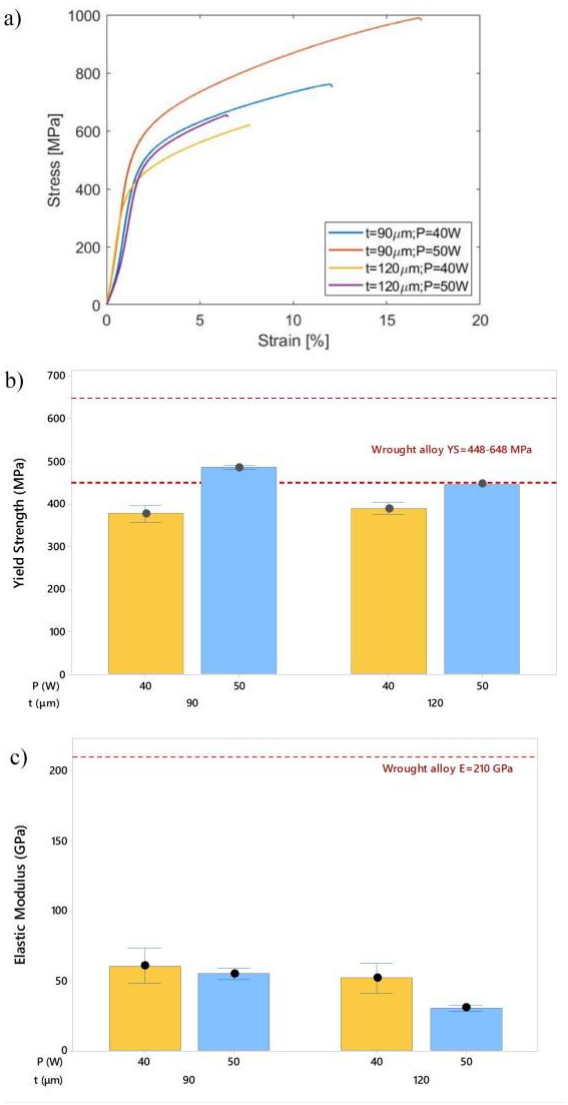


Figure 13. a) Typical stress-strain curves of micro SLM produced specimens subjected to tensile testing (note that t=120 μm conditions did not reach UTS, since the maximum static force of the machine was reached) and b) effect of laser power and strut thickness on yield strength (YS) and c) elastic modulus (E) (error bars indicate standard error).

Table 3. Mechanical properties of the SLM produced struts compared to the wrought CoCr alloy.

| **Condition** | **t=90 μm, P=40 W** | **t=90 μm, P=50 W** | **t=120 μm, P=40 W** | **t=120 μm, P=50 W** | **Wrought L605** [53,54] |
|---|---|---|---|---|---|
| E [GPa] | 60.4 ± 12.7 | 54.9 ± 3.9 | 52.1 ± 10.5 | 30.3 ± 2.3 | 243 |
| YS [MPa] | 376.5 ± 82.0 | 485.1 ± 21.1 | 388.7 ± 43.3 | - | 448–648 |
| UTS [Mpa] | 694.0 ± 31.3 | 983.9 ± 4.3 | - | - | 951–1220 |
| $\varepsilon_f$ [%] | 9.9 ± 1.2 | 16.2 ± 0.3 | - | - | 50-60 |

### 4.5. Expansion behaviour

In Figure 14 an example of a stent during its expansion at different pressure values is reported. The diameter of as-built and electropolished stents as a function of pressure is shown in Figure 15.a-b. The behaviour is similar for all the stents and there were no evident cracks. The expansion behaviour in terms of expansion ratio is reported in

Figure 15.c-d for the stents in both the investigated conditions. Looking at the expansion ratio trend, it appears that the internal diameter of the stents both in as-built condition and after electropolishing increased more than twice the initial value. In as-built conditions, the expansion ratio appears to depend on the process parameters, while after electrochemical polishing such differences is not visible. This can be attributed to the fact that after electrochemical polishing the strut sizes are similar in each condition. A SEM image of a connection between struts after expansion is reported in Figure 16. It can be seen that the expanded stents are free of defects and cracks, both in the as-built condition (Figure 16.a) and after electropolishing (Figure 16.b).

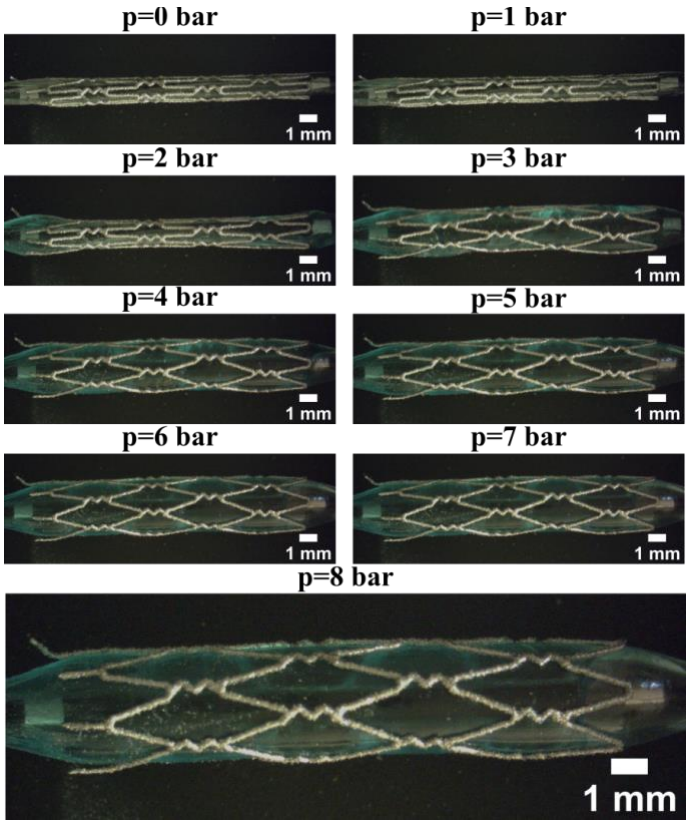

Figure 14. Images of an SLM stent (t=90µm; P=50 W) expanded from 0 to 8 bar.

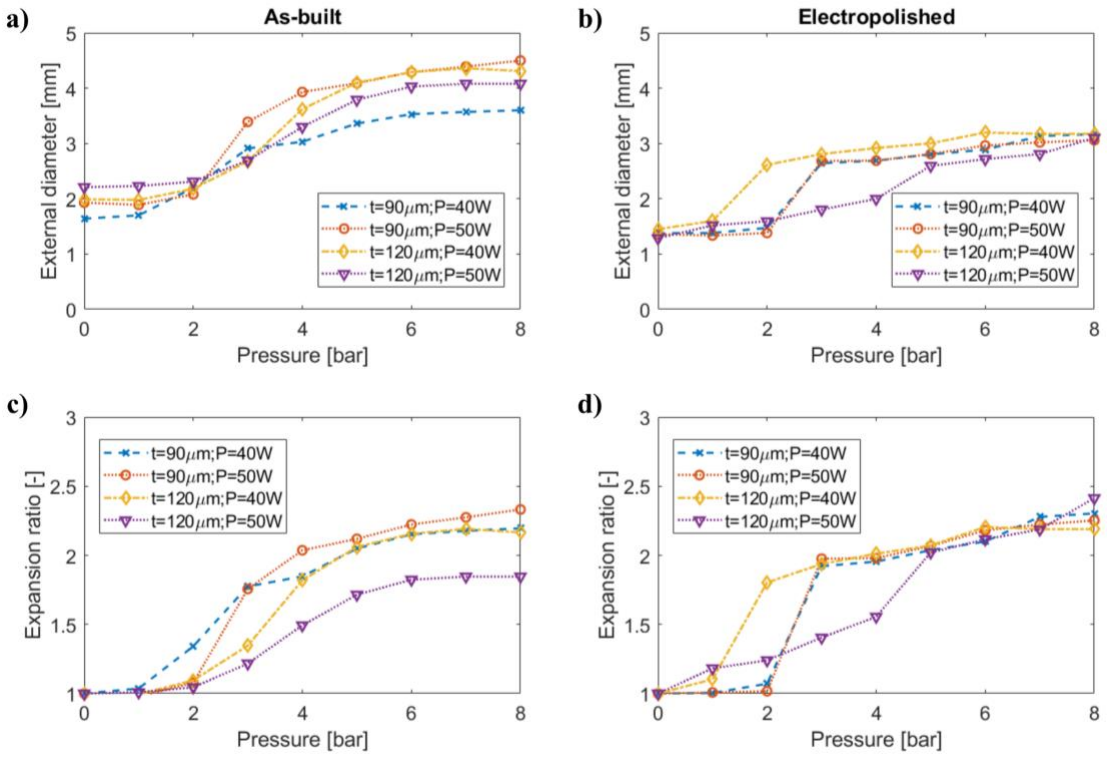


Figure 15. Expansion behaviour of as-built and electropolished stents in terms of external diameter dependence on pressure (a and b) and expansion ratio (c and d). Standard error not shown due to the small values not visible under the indicators.

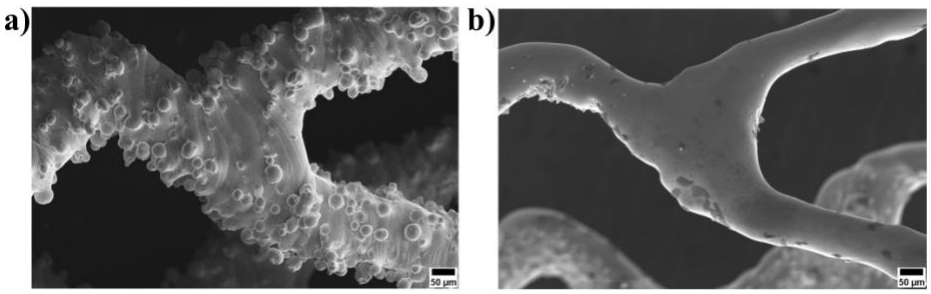


Figure 16. SEM image of a stent connection after expansion a) in the as-built and b) electropolished condition (P=50W, t=90 µm).

## 5. Discussion

Several factors determine the functionality of a stent concerning the mesh design, manufacturing cycle, and the mechanical properties. The mesh employed in this work is constrained by the design rules of the SLM process. The results show that with adequate design choices a functional stent is achievable. However, concerning the stent design several points remain open. The conventional CoCr stents employed are characterized by open cells and thin struts. The feasibility of producing open celled stents is an open point for future investigations. The produced stents deviated significantly from the nominal strut section geometry. In a previous work, authors demonstrated reasonable geometrical fidelity with thicker struts (>300 µm) [16]. Evidently, smaller struts, which require fewer

laser pulses, deviate more easily from the strut section. This can be attributed to the formation of a continuous and large melt pool, which forms a circular shape due to the surface tensions involved. Indeed, melt pool area can be comparable to the strut sizes even at PW emission [28]. Accordingly, the strut section should be designed following the design rules of the SLM process. The mesh projection to a tubular surface is indeed adequate for laser cutting, which is the conventional stent manufacturing process.

In this work, the materials were tested in as-built conditions, while the CoCr alloys can be heat treated for solution treatment for improving elongation at break. The material properties obtained are comparable to solution treated CoCr alloy produced by SLM as reported by Sing et al [55]. The authors applied solution treatment at 1220°C for variable duration of 1, 2, and 4 h. The as-built specimens showed approximately UTS=1100 MPa, YS=900 MPa and $\varepsilon_f$=5%. After an hour of solution treatment, the YS was reduced to approximately 500 MPa and UTS to 600 MPa while improving the elongation to 10%. Aging treatment can also be applied to increase UTS with the expense of a more fragile rupture [56]. The pulsed emission profile along with the very thin struts are likely to induce cooling conditions much different from large parts produced by CW emission reported in literature. Hence, it can be deduced that the SLM processing conditions can be potentially adapted to achieve the required strength without the necessity to apply further heat treatment for producing stents. However, the influence of the layered production and anisotropy of the material properties on the fatigue properties should still be assessed.

The comparison of the mechanical properties against the conventional L605 shown in Table 3 depicts that the SLM produced CoCr struts are comparable overall to the conventional alloy. The main difference is observed at the low elastic modulus of the SLM produced struts. This can be associated to a size effect, which has been previously reported in literature [57,58]. However, the observed reduction of the elastic modulus in this work is much higher than the values observed by the previous works. The mechanisms behind concerning the size effect are still under investigation. A lower elastic modulus with the same strut thickness implies a lower radial stiffness of the stent. This might result in a not sufficient radial force applied by the stent to the vessel, which requires further investigations. The stent material requires a sufficient UTS level to avoid rupture. An adequate YS level is required on the other hand to avoid plasticization prior to deployment. The elongation at rupture is also an

important indicator to how much the stent can be deformed to the final form before the failure. In the tested conditions, the elongation was found to be smaller than the conventional material properties, indicating lower ductility. The balance between these parameters ensure the correct deployment as well as functioning throughout the lifetime of the device. The results show that the SLM produced stents are promising in terms of their mechanical properties as their balloon expandability has been confirmed. Indeed, the balloon expansion stage is one of the most critical points in the lifetime of the cardiovascular stents.

## 6. Conclusions

This work reports additive manufacturing, finishing, and functional characterization of CoCr cardiovascular stents with a novel mesh designed for SLM. The stents were successfully produced and their expansion was assessed using a balloon catheter. No support structures were used and stents were realized with different process parameters. In all the configurations the stents were produced with a high geometrical fidelity. The main outcomes of the work can be summarized as follow.

- Adequate mesh design allows for producing balloon expandable stents without internal or external defects after production and after expansion.
- Concerning the small size of the devices to be produced, the strut thickness becomes a process parameter to be evaluated along with the laser related parameters.
- Electrochemical polishing is effective in reducing the surface roughness by approximately 80%. However, the surface roughness should be further reduced to fit the requirements of biomedical devices. Combination of different finishing processes can be envisaged for a more effective post-processing stage.
- In order to maintain the desired strut thickness and shape the SLM and electropolishing stages should be considered together. Although, the SLM process produces stents with larger struts, by the end of the electropolishing stage the strut size can be smaller than the nominal one. The overall strut allowance should be calculated considering the complete production chain.

- The mechanical properties of the material depend also on the processing strategy. This can be further exploited to tailor the device properties as well as avoid heat treatment stages common to SLM produced larger components.
- Expansion behaviour of the stents were found to depend on the processing conditions in as-built conditions, presumably due to the differences in the strut size. After electrochemical polishing, the strut thicknesses became comparable and the expansion ratios were similar.

The present results shed light on the potential of producing cardiovascular stents via SLM. Several research themes open up related to the progression of this new manufacturing approach. Topological optimization tools can be employed to optimize the expansion behaviour of stent as well as its fatigue resistance. The biological performance of the materials produced with the new technology should also be addressed.

## References


[1] Wilkins E, Wilson L, Wickramasinghe K, Bhatnagar P, Leal J, Luengo-Fernandez R, et al. European Cardiovascular Disease Statistics 2017. European Heart Network; 2017.

[2] Torii S, Jinnouchi H, Sakamoto A, Kutyna M, Cornelissen A, Kuntz S, et al. Drug-eluting coronary stents: insights from preclinical and pathology studies. Nat Rev Cardiol 2019:1. doi:10.1038/s41569-019-0234-x.

[3] Rebagay G, Bangalore S. Biodegradable Polymers and Stents: the Next Generation? Curr Cardiovasc Risk Rep 2019;13:22. doi:10.1007/s12170-019-0617-x.

[4] Berti F, Spagnoli A, Petrini L. A numerical investigation on multiaxial fatigue assessment of Nitinol peripheral endovascular devices with emphasis on load non-proportionality effects. Eng Fract Mech 2019:106512. doi:10.1016/J.ENGFRACMECH.2019.106512.

[5] O'Brien B, Zafar H, Ibrahim A, Zafar J, Sharif F. Coronary Stent Materials and Coatings: A Technology and Performance Update. Ann Biomed Eng 2016;44:523–35. doi:10.1007/s10439-015-1380-x.

[6] Stoeckel D, Bonsignore C, Duda S, Dunitz M. A survey of stent designs. Minim Invasive Ther Allied Technol 2002;11:137–47. doi:10.1080/136457002760273340.

[7] Demir AG, Previtali B. Comparative study of CW, nanosecond- and femtosecond-pulsed laser microcutting of AZ31 magnesium alloy stents. Biointerphases 2014;9:029004. doi:10.1116/1.4866589.

[8] Finazzi V, Demir AG, Biffi CA, Chiastra C, Migliavacca F, Petrini L, et al. Design Rules for Producing Cardiovascular Stents by Selective Laser Melting: Geometrical Constraints and Opportunities. Procedia Struct Integr 2019;15:16–23. doi:10.1016/j.prostr.2019.07.004.

[9] Catalano G, Demir AG, Furlan V, Previtali B. Prototyping of biodegradable flat stents in pure zinc by laser microcutting and chemical etching. J Micromechanics Microengineering 2018;28:095016. doi:10.1088/1361-6439/aac83d.

[10] Guerra AJ, Ciurana J. 3D-printed bioabsordable polycaprolactone stent: The effect of process parameters on its physical features. Mater Des 2018;137:430–7. doi:10.1016/j.matdes.2017.10.045.

[11] van Lith R, Baker E, Ware H, Yang J, Farsheed AC, Sun C, et al. 3D-Printing Strong High-Resolution Antioxidant Bioresorbable Vascular Stents. Adv Mater Technol 2016;1:1600138. doi:10.1002/admt.201600138.

[12] Misra SK, Ostadhossein F, Babu R, Kus J, Tankasala D, Sutrisno A, et al. 3D-Printed Multidrug-Eluting Stent from Graphene-Nanoplatelet-Doped Biodegradable Polymer Composite. Adv Healthc Mater 2017;6:1700008. doi:10.1002/adhm.201700008.

[13] Flege C, Vogt F, Hoeges S, Jauer L, Borinski M, Schulte VA, et al. Development and characterization of a coronary polylactic acid stent prototype generated by selective laser melting. J Mater Sci Med 2013;24:241–55. doi:10.1007/s10856-012-4779-z.

[14] Park SA, Lee SJ, Lim KS, Bae IH, Lee JH, Kim WD, et al. In vivo evaluation and characterization of a bio-absorbable drug-coated stent fabricated using a 3D-printing system. Mater Lett 2015;141:355–8. doi:10.1016/J.MATLET.2014.11.119.

[15] Zhao D, Zhou R, Sun J, Li H, Jin Y. Experimental study of polymeric stent fabrication using homemade 3D printing system. Polym Eng Sci 2019;59:1122–31. doi:10.1002/pen.25091.

[16] Demir AG, Previtali B. Additive manufacturing of cardiovascular CoCr stents by selective laser melting. Mater Des 2017;119:338–50. doi:10.1016/j.matdes.2017.01.091.

[17] Wessarges Y, Hagemann R, Gieseke M, Nölke C, Kaierle S, Schmidt W, et al. Additive manufacturing of vascular implants by selective laser melting. Biomed Tech 2014;59:S404. doi:10.1515/bmt-2014-5005.

[18] Wen P, Voshage M, Jauer L, Chen Y, Qin Y, Poprawe R, et al. Laser additive manufacturing of Zn metal parts for biodegradable applications: Processing, formation quality and mechanical properties. Mater Des 2018;155:36–45. doi:10.1016/J.MATDES.2018.05.057.

[19] Schofield K, Sydneia A, Arcuri A, Bulcão R, Nascimento S, Schofield E, et al. Nanotoxicology and Exposure in the Occupational Setting 2015;3:35–48. doi:10.4236/odem.2015.33005.

[20] Yan C, Hao L, Hussein A, Raymont D. Evaluations of cellular lattice structures manufactured using selective laser melting. Int J Mach Tools Manuf 2012;62:32–8. doi:10.1016/j.ijmachtools.2012.06.002.

[21] Yan C, Hao L, Hussein A, Young P, Raymont D. Advanced lightweight 316L stainless steel cellular lattice structures fabricated via selective laser melting. Mater Des 2014;55:533–41. doi:10.1016/j.matdes.2013.10.027.

[22] Qiu C, Yue S, Adkins NJE, Ward M, Hassanin H, Lee PD, et al. Influence of processing conditions on strut structure and compressive properties of cellular lattice structures fabricated by selective laser melting. Mater Sci Eng A 2015;628:188–97. doi:10.1016/j.msea.2015.01.031.

[23] Leary M, Mazur M, Elambasseril J, McMillan M, Chirent T, Sun Y, et al. Selective laser melting (SLM) of AlSi12Mg lattice structures. Mater Des 2016;98:344–57. doi:10.1016/J.MATDES.2016.02.127.

[24] Choy SY, Sun C-N, Leong KF, Wei J. Compressive properties of functionally graded lattice structures manufactured by selective laser melting. Mater Des 2017;131:112–20. doi:10.1016/J.MATDES.2017.06.006.

[25] Carluccio D, Xu C, Venezuela J, Cao Y, Kent D, Bermingham M, et al. Additively manufactured iron-manganese for biodegradable porous load-bearing bone scaffold applications. Acta Biomater 2020;103:346–60. doi:10.1016/j.actbio.2019.12.018.

[26] Caprio L, Demir AG, Previtali B. Influence of pulsed and continuous wave emission on melting efficiency in selective laser melting. J Mater Process Tech 2018;266:429–41. doi:10.1016/j.jmatprotec.2018.11.019.

[27] Caprio L, Demir AG, Previtali B. Comparative study between CW and PW emissions in selective laser melting. J Laser Appl 2018;30:032305. doi:10.2351/1.5040631.

[28] Demir AG, Mazzoleni L, Caprio L, Pacher M, Previtali B. Complementary use of pulsed and continuous wave emission modes to stabilize melt pool geometry in laser powder bed fusion. Opt Laser Technol 2019;113:15–26. doi:10.1016/j.optlastec.2018.12.005.

[29] Ren L, Memarzadeh K, Zhang S, Sun Z, Yang C, Ren G, et al. A novel coping metal material CoCrCu alloy fabricated by selective laser melting with antimicrobial and antibiofilm properties. Mater Sci Eng C 2016;67:461–7. doi:10.1016/j.msec.2016.05.069.

[30] Schwindling FS, Seubert M, Rues S, Koke U, Schmitter M, Stober T. Two-Body Wear of CoCr Fabricated by Selective Laser Melting Compared with Different Dental Alloys. Tribol Lett 2015;60:1–8. doi:10.1007/s11249-015-0601-7.

[31] Sidambe AT. Effects of build orientation on 3D-printed Co-Cr-Mo: surface topography and L929

fibroblast cellular response. Int J Adv Manuf Technol 2018;99:867–80. doi:10.1007/s00170-018-2473-0.

[32] Cutolo A, Neirinck B, Lietaert K, de Formanoir C, Van Hooreweder B. Influence of layer thickness and post-process treatments on the fatigue properties of CoCr scaffolds produced by laser powder bed fusion. Addit Manuf 2018;23:498–504. doi:10.1016/J.ADDMA.2018.07.008.

[33] Caravaggi P, Liverani E, Leardini A, Fortunato A, Belvedere C, Baruffaldi F, et al. CoCr porous scaffolds manufactured via selective laser melting in orthopedics: Topographical, mechanical, and biological characterization. J Biomed Mater Res Part B Appl Biomater 2019. doi:10.1002/jbm.b.34328.

[34] Lu Y, Ren L, Wu S, Yang C, Lin W, Xiao S, et al. CoCrWCu alloy with antibacterial activity fabricated by selective laser melting: Densification, mechanical properties and microstructural analysis. Powder Technol 2018;325:289–300. doi:10.1016/J.POWTEC.2017.11.018.

[35] Seyedi M, Zanotto F, Monticelli C, Balbo A, Liverani E, Fortunato A. Microstructural characterization and corrosion behaviour of SLM CoCrMo alloy in simulated body fluid. Metall Ital 2018;110:45–50.

[36] Xin X, Xiang N, Chen J, Xu D, Wei B. Corrosion characteristics of a selective laser melted Co  Cr dental alloy under physiological conditions. J Mater Sci 2012;47:4813–20. doi:10.1007/s10853-012-6325-2.

[37] Hooreweder B Van, Lietaert K, Neirinck B, Lippiatt N, Wevers M. CoCr F75 scaffolds produced by additive manufacturing: Influence of chemical etching on powder removal and mechanical performance. J Mech Behav Biomed Mater 2017;70:60–7. doi:10.1016/J.JMBBM.2017.03.017.

[38] Strano G, Hao L, Everson RM, Evans KE. Surface roughness analysis, modelling and prediction in selective laser melting. J Mater Process Technol 2013;213:589–97. doi:10.1016/j.jmatprotec.2012.11.011.

[39] Baicheng Z, Xiaohua L, Jiaming B, Junfeng G, Pan W, Chen-nan S, et al. Study of selective laser melting (SLM) Inconel 718 part surface improvement by electrochemical polishing. Mater Des 2017;116:531–7. doi:10.1016/J.MATDES.2016.11.103.

[40] Anilli M, Demir AG, Previtali B. Additive manufacturing of laser cutting nozzles by SLM: processing, finishing and functional characterization. Rapid Prototyp J 2018;24. doi:10.1108/RPJ-05-2017-0106.

[41] Demir AG, Previtali B, Biffi CA. Fibre laser cutting and chemical etching of AZ31 for manufacturing biodegradable stents. Adv Mater Sci Eng 2013;2013. doi:10.1155/2013/692635.

[42] Zeidler H, Nestler K, Böttger-Hiller F, Schubert A, Previtali B, Demir AG. Finishing of laser-machined coronary stents by plasma electrolytic polishing. Proc. 16th Int. Conf. Eur. Soc. Precis. Eng. Nanotechnology, EUSPEN 2016, 2016.

[43] Gebhardt A, Hötter J-S, Ziebura D. Impact of SLM build parameters on the surface quality. RTejournal - Forum Für Rapid Technol 2014;2014.

[44] Murphy BP, Savage P, McHugh PE, Quinn DF. The Stress–Strain Behavior of Coronary Stent Struts is Size Dependent. Ann Biomed Eng 2003;31:686–91. doi:10.1114/1.1569268.

[45] Hanzl P, Zetek M, Bakša T, Kroupa T. The Influence of Processing Parameters on the Mechanical Properties of SLM Parts. Procedia Eng 2015;100:1405–13. doi:10.1016/J.PROENG.2015.01.510.

[46] Koutsoukis T, Zinelis S, Eliades G, Al-Wazzan K, Rifaiy MA, Jabbari YS Al. Selective Laser Melting Technique of Co-Cr Dental Alloys: A Review of Structure and Properties and Comparative Analysis with Other Available Techniques. J Prosthodont 2015;24:303–12. doi:10.1111/jopr.12268.

[47] Demir AG, Colombo P, Previtali B. From pulsed to continuous wave emission in SLM with contemporary fiber laser sources: effect of temporal and spatial pulse overlap in part quality. Int J Adv Manuf Technol 2017;91:2701–14. doi:10.1007/s00170-016-9948-7.

[48] Carluccio D, Demir AG, Caprio L, Previtali B, Bermingham MJ, Dargusch MS. The influence of laser processing parameters on the densification and surface morphology of pure Fe and Fe-35Mn scaffolds produced by selective laser melting. J Manuf Process 2019;40:113–21. doi:10.1016/j.jmapro.2019.03.018.

[49] Spierings AB, Levy G. Comparison of density of stainless steel 316L parts produced with selective laser melting using different powder grades. Proc. Solid Free. Fabr. Symp., 2009, p. 342–53.

[50] Townsend A, Senin N, Blunt L, Leach RK, Taylor JS. Surface texture metrology for metal additive manufacturing: a review. Precis Eng 2016;46:34–47. doi:10.1016/j.precisioneng.2016.06.001.

[51] Mergulhão MV, Podestá CE, das Neves MDM. Mechanical Properties and Microstructural Characterization of Cobalt-Chromium (CoCr) Obtained by Casting and Selective Laser Melting (SLM). Mater Sci Forum 2017;899:534–9. doi:10.4028/www.scientific.net/MSF.899.534.

[52] Poncin P, Proft J. Stent Tubing: Understanding the Desired Attributes. Proc ASM Conf Mater Process Med Devices 2003:253–9.

[53] Mani G, Feldman MD, Patel D, Agrawal CM. Coronary stents: a materials perspective. Biomaterials 2007;28:1689–710. doi:10.1016/j.biomaterials.2006.11.042.

[54] Sweeney CA, O'Brien B, McHugh PE, Leen SB. Experimental characterisation for micromechanical modelling of CoCr stent fatigue. Biomaterials 2014;35:36–48. doi:10.1016/j.biomaterials.2013.09.087.

[55] Sing SL, Huang S, Yeong WY. Effect of solution heat treatment on microstructure and mechanical properties of laser powder bed fusion produced cobalt-28chromium-6molybdenum. Mater Sci Eng A 2020;769:138511. doi:10.1016/j.msea.2019.138511.

[56] Zhang M, Yang Y, Song C, Bai Y, Xiao Z. An investigation into the aging behavior of CoCrMo alloys fabricated by selective laser melting. J Alloys Compd 2018;750:878–86. doi:10.1016/j.jallcom.2018.04.054.

[57] Liang H, Xie D, Mao Y, Shi J, Wang C, Shen L, et al. The size effect on forming quality of Ti–6Al–4V solid struts fabricated via laser powder bed fusion. Metals (Basel) 2019;9. doi:10.3390/met9040416.

[58] Gavazzoni M, Boniotti L, Foletti S. Influence of specimen size on the mechanical properties of microlattices obtained by selective laser melting. Proc Inst Mech Eng Part C J Mech Eng Sci 2019;0:1–14. doi:10.1177/0954406219869741.

**List of tables**

## List of figures